

Optical control of entangled states in quantum wells

E. Räsänen,^{1,2,3,*} T. Blasi,^{3,4} M. F. Borunda,^{3,5} and E. J. Heller^{3,6}

¹*Department of Physics, Tampere University of Technology, FI-33101 Tampere, Finland*

²*Nanoscience Center, Department of Physics, University of Jyväskylä, FI-40014 Jyväskylä, Finland*

³*Physics Department, Harvard University, Cambridge, Massachusetts 02138, USA*

⁴*Physik Department, Technische Universität München, D-85747 Garching, Germany*

⁵*Department of Physics, Oklahoma State University, Stillwater, Oklahoma 74078, USA*

⁶*Department of Chemistry and Chemical Biology, Harvard University, Cambridge, Massachusetts 02138, USA*

(Dated: May 22, 2018)

We present theory and calculations for coherent high-fidelity quantum control of many-particle states in semiconductor quantum wells. We show that coupling a two-electron double quantum dot to a terahertz optical source enables targeted excitations that are one to two orders of magnitude faster and significantly more accurate than those obtained with electric gates. The optical fields subject to physical constraints are obtained through quantum optimal control theory that we apply in conjunction with the numerically exact solution of the time-dependent Schrödinger equation. Our ability to coherently control arbitrary two-electron states, and to maximize the entanglement, opens up further perspectives in solid-state quantum information.

PACS numbers: 78.67.Hc, 73.21.La, 78.20.Bh, 03.67.Bg

Quest for solid-state quantum computing^{1,2} in low-dimensional semiconductor materials has led to experimental breakthroughs in the initialization, processing, and readout of single- and two-particle states in coupled quantum dots.^{3–6} The majority of proposed quantum computation schemes focus on spin control⁷ due to the long decoherence times up to microseconds. However, rapid development of light sources and ultrafast science in atomic physics⁸ is likely to bring methods and techniques to coherent control of electric charge⁹ in low-dimensional systems.

Electron dynamics in double quantum dots (DQDs) has been subject to various theoretical approaches. Beyond few-level models, realistic DQDs have been controlled with gate voltages^{10,11,13} and optimized laser pulses.^{14–17} Murgida and co-workers^{10,11} presented an scheme to reach desired excited states in two-electron DQDs by “navigating” in the energy spectrum with electric fields – an approach widely used for two- and three-level systems.¹² Here we focus on a similar quasi-one-dimensional setup and show that optical fields can lead to almost 100% fidelities of targeted entangled two-electron states in tens of picoseconds, thus improving *both* the operation time and the fidelity from earlier works by 1-2 orders of magnitude. In this context, we extend the previous single-particle^{14,15} and two-particle^{16,17} optimization studies into an all-round scheme to coherently control an arbitrary transition in a two-electron DQD. Moreover, we show that the control procedure validates for the maximization of the entanglement itself, which might have further implications for quantum information in solid-state devices.

Our model system is illustrated in Fig. 1(a). We consider a quasi-one-dimensional nanowire fabricated, e.g., by epitaxial methods.¹⁸ Two QDs are separated by tunnel barriers, and the strength and position of the central

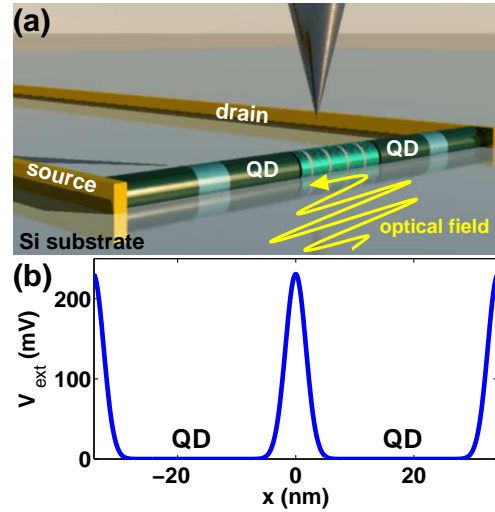


FIG. 1: (color online) (a) Schematic picture of the proposed setup. Two quantum dots in a quasi-one-dimensional nanowire are separated by tunnel barriers, and the central one can be adjusted by a conducting tip. (b) One-dimensional model potential for a double quantum dot used in the calculations.

barrier can be adjusted by a scanning gate microscope tip.^{19,20} Here we assume the tip to be located in the middle, so that the one-dimensional model potential has the shape shown in Fig. 1(b). The edges of the barriers are softened by Gaussian functions.

For general applicability of our results, and to explicitly compare with Refs. 10 and 11, we consider GaAs material parameters with the effective mass $m^* = 0.067 m_e$ and dielectric constant $\epsilon = 12.4 \epsilon_0$. We use effective atomic units (a.u.) throughout the paper apart from the physical model in Fig. 1(b). The energies, lengths,

and times scale as $E_h^* = (m^*/m_0)/(\epsilon/\epsilon_0)^2 E_h \approx 11$ meV, $a_0^* = (\epsilon/\epsilon_0)/(m^*/m_0) a_0 \approx 10$ nm, and $t_0^* = \hbar/E_h^* \approx 55$ fs, respectively.

The two-electron problem in one dimension is solved numerically exactly by considering electron coordinates x_1 and x_2 and a soft-Coulomb interaction of the form $V_{\text{int}}(x_1, x_2) = [(x_1 - x_2)^2 + \alpha]^{-1/2}$ with a softening parameter $\alpha = 0.25$. The Hamiltonian reads $H = K + V_{\text{ext}}(x_1, x_2) + V_{\text{int}}(x_1, x_2) - \mu\epsilon(t)$, where K is the kinetic-energy operator and $V_{\text{ext}}(x_1, x_2) = \max[V(x_1), V(x_2)]$ with $V(x_i)$ is the external confinement potential for each individual electron shown in Fig. 1(b). It represents a double quantum well with a depth 220 meV, width 35 nm, and interwell barrier 5 nm. In the Hamiltonian $\hat{\mu} = -e(x_1, x_2)$ is the dipole operator and $\epsilon(t)$ is the optical field. We point out that the spatial wave functions across the diagonal $x_1 = x_2$ are symmetric, since we consider only antisymmetric two-electron singlet states (so that the total wave function is antisymmetric). We could focus on triplets in a similar manner by considering only spatially antisymmetric wave functions. A small distortion potential $V_d(x_1, x_2) = 0.001(x_1 + x_2)$, corresponding to a small static field, is added to the Hamiltonian to distinguish degenerate eigenstates as in a real setup, where impurities are always present.

Our task is to *optimize* $\epsilon(t)$ such that the two-electron wave function $|\Psi(x_1, x_2)\rangle$ reaches the desired target state $|\Phi_F\rangle$ at a fixed time T by maximizing the overlap $|\langle\Psi(x_1, x_2, T)|\Phi_F\rangle|^2$. To this end, we apply quantum optimal control theory²¹ (OCT) as explained in Ref. 15. This gives the optimized field $\epsilon(t)$ through an iterative procedure of the time-dependent Schrödinger equation. As physical constraints, we set the maximum allowed frequency in the field to ω_{max} and the fluence F , i.e., the integrated intensity (values given below). We use the OCT scheme of Werschnik and Gross²² and apply the octopus code²³ in real space and real time.

First we consider an excitation where the electrons stay in separate dots (we call this a delocalized configuration) but a node is created in both dots as shown in the inset of Fig. 2. This corresponds to an excitation from the ground state $|1\rangle$ to the fourth state $|4\rangle$ ($|2\rangle$ and $|3\rangle$ are localized configurations with both electrons being in the left and right well, respectively) The obtained yield strongly depends on ω_{max} allowed in the optimization, and with a pulse length $T = 300$ (17 ps) we find a strong increase slightly above $\omega_{\text{max}} = 1.4$. This is simply due to the resonance at $E_4 - E_1 = 1.3957$ (dashed line), which is a crucial frequency to be included in the optimization to reach extremely high yields. A shorter ($T = 100$) but more intensive pulse lacks this behavior due to the tunneling character of the excitation; the Keldysh parameter – used in atoms to assess whether the process is of tunneling or (multi)photon character – is inversely proportional to the peak intensity.²⁴ However, the shorter pulse leads to higher yields than the longer (and less intensive) one with filter frequencies smaller than the resonance frequency. To underline the effectiveness of OCT in Fig. 2

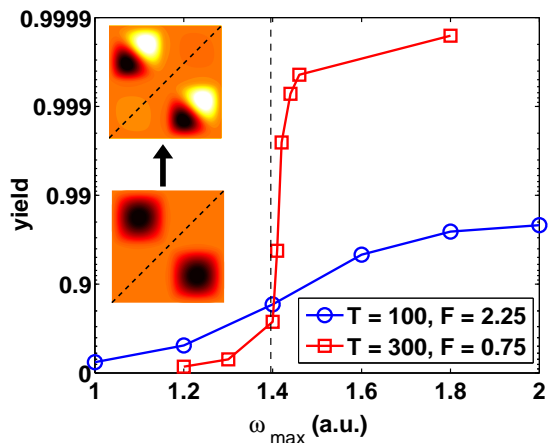


FIG. 2: (color online) Yield as a function of the maximum frequency in the optimized pulse to excite the system from the ground state to the fourth state. The electrons remain delocalized but a node is created in the wells (see the inset). Two different pulse lengths and fluences are considered (see text).

it is noteworthy that a *non-optimized* pulse with the resonant frequency and $T = 100$ and $T = 300$, leads, *at most*, to yields $\sim 70\%$ and $\sim 95\%$, respectively, whereas the optimized pulses, with ω_{max} about 10% above the resonance, lead to respective yields of $\sim 95\%$ and $\sim 99.95\%$.

In Fig. 3 we show our results for an optimized excitation from the ground state $|1\rangle$ to a superposition that consists of the six lowest states, i.e., the target state can be written as $|\Phi_F\rangle = (1/\sqrt{6})(|1\rangle + |2\rangle + |3\rangle + |4\rangle + |5\rangle + |6\rangle)$ [Fig. 3(a)]. The pulse length and fluence are fixed to $T = 600$ ($= 33$ ps) and $F = 6$ ($= 71$ meV), respectively, and the filter frequency is $\omega_F = 3$ ($= 8.6$ THz). As shown in Fig. 3(b) we find an extremely high total yield 99.6%, and the occupations of the individual states converge close to 1/6 (see the inset). The final density, consisting of both localized and delocalized contributions, is shown in the right inset.

It was shown in Ref. 11 that properly adjusted electric fields can drive a similar system to a three-state superposition in 1000 ps with 96.56% final overlap. In this respect, our optical scheme appears to be about 30 times faster and an order of magnitude more accurate, even though the target system is more complex (six states instead of three). The price to pay is the rather complicated control field in Fig. 3(c) that, however, satisfies realistic constraints and, secondly, can be thoroughly understood with the following analysis. It is important to note that the optimized field as the one in Fig. 3(c) corresponds to a *local* maximum in a search space, i.e., there might be other solutions yielding similar, or even better outcomes.

Figure 4 shows a time-frequency map of the optimized pulse in Fig. 3(c). The amplitudes of the appearing frequencies (y axis) during the pulse (x axis) are shown

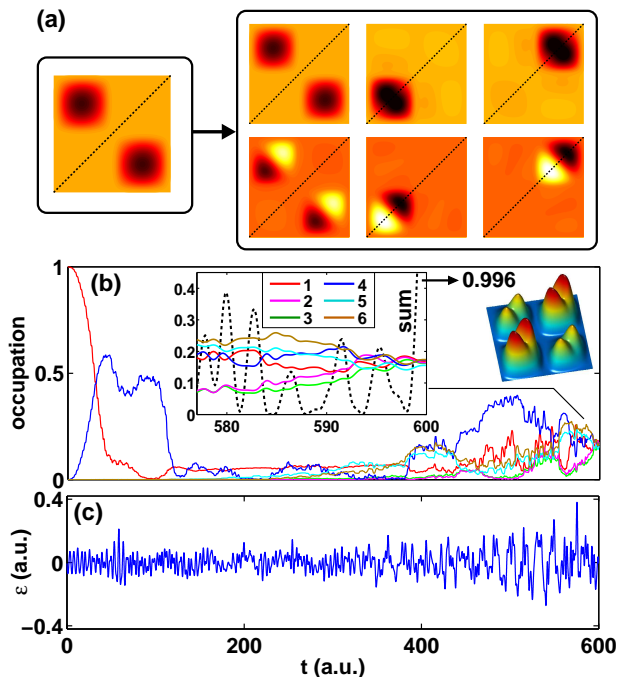


FIG. 3: (color online) (a) Excitation process from the ground state to an equal superposition of six eigenstates. (b) Occupations of the states during the optimized process. At the end (inset) the states reach $\sim 1/6$ occupations while a total yield of 99.6% is obtained for the superposition (total density shown in the right inset). (c) Optimized pulse analyzed in Fig. 4.

in colorscale. Time frames of $\Delta t = T/10 = 60$ were used in the Fourier transforms. Several distinctive features can be seen in the map, and they can be associated with specific (de)excitation processes. First, in the beginning of the pulse we find pronounced frequencies around $\omega \sim 1.5$ and 2.4 corresponding to *delocalized* excitations, i.e., nodes are created in left-right configurations, with $\omega_{1,4} = E_4 - E_1 = 1.40$ (as in Fig. 2), $\omega_{4,7} = 1.43$, and $\omega_{4,10} = 2.30$. Around $t = 400 \dots 500$ we find similar processes for *localized* configurations (left-left or right-right) with $\omega_{2,5} = \omega_{3,6} = 1.57$ and $\omega_{5,8} = \omega_{6,9} = 1.06$. In between, we find contributions corresponding to *transitions* between delocalized and localized configurations. They occur through superpositions of the localized states and require frequencies equal to energy gaps between delocalized and localized states. Finally, close to the end of the pulse we find a very large amplitude at $\omega \sim 0.5$ alongside several small-scale features. They correspond to several *deexcitations* from high-lying occupations back to the target eigenstates as discussed within Fig. 3. Overall, with the time-frequency map we are able to understand most features of the optimization process despite the complicated shape of the pulse in the time domain [Fig. 3(c)]. On the basis of Fig. 2 it can be expected that filtering out the dominating frequencies in Fig. 4 may significantly lower the yield. Quantitative assessment of the sensitivity of the yield to different frequencies is the subject of

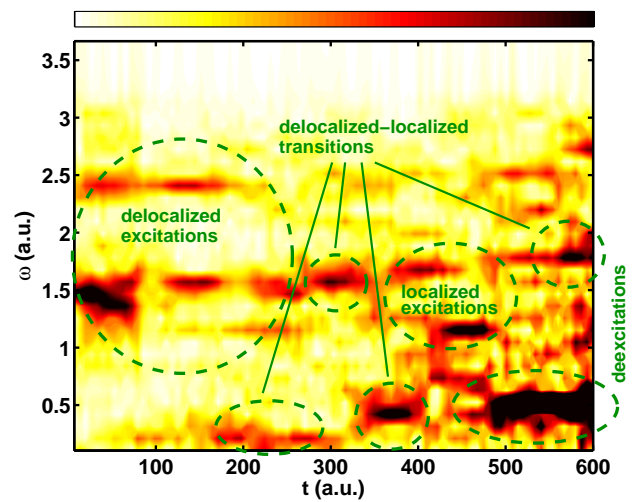


FIG. 4: (color online) Time-frequency map of the optimized field shown in Fig. 3(c). Amplitudes of the appearing frequencies as a function of time are shown in colorscale (white: small, black: large). Several (de)excitation processes can be distinguished (see text).

future work.

Finally, we examine how the correlation entropy and entanglement are evolved during the controlled excitation to a superposition. The correlation entropy^{25,26} is defined as $S = -\sum_k^N n_k \ln n_k$, where the sum runs over the N lowest eigenvalues n_k of the one-body density matrix. The maximum value for S is obtained when $n_k = 1/N$, i.e., when all the states are equally occupied.

The entanglement, on the other hand, is defined here in terms of the von Neumann entropy²⁷ $E_j = -\text{Tr}(\rho_j \log_2 \rho_j)$, where $\rho_j = \text{Tr}_j(|\Psi\rangle\langle\Psi|)$ is the reduced density matrix, and the trace is taken over the j :th site (1 or 2) of the DQD. The three possible well occupations are $|q\rangle_j$ with $q = 0, 1, 2$ being the charge of the well. Now the reduced density matrix becomes $\rho_j = p_{0,j}|0\rangle_j\langle 0|_j + p_{1,j}|1\rangle_j\langle 1|_j + p_{2,j}|2\rangle_j\langle 2|_j$ (occupations $|1\rangle_j$ and $|2\rangle_j$ should not be mixed with *states* $|1\rangle$ and $|2\rangle$). Here $p_{i,j}$ is the probability of the j th site being occupied with i electrons. Therefore, the entanglement can be written as $E_j = \sum_{i=0}^2 p_{i,j} \log_2 p_{i,j}$.

In Fig. 5 we plot the correlation entropy (upper panel) and the entanglement (lower panel) for two excitations: from the ground state to the superposition of the first three states, i.e., $|\Phi_F\rangle = (1/\sqrt{3})(|1\rangle + |2\rangle + |3\rangle)$, and to the superposition to the first six states (the same as in Figs. 3 and 4). The correlation entropy oscillates strongly in both cases but eventually reaches the values 1.1112 and 1.8062, respectively, that are very close to the ideal values $\ln(3) \approx 1.0986$ and $\ln(6) \approx 1.7918$ (dotted lines). This means that at $t = T$ the eigenstates in the target superpositions are almost equally occupied. The higher entropies at $t < T$ are due to the distribution of the electron occupations to a large number of states – about 20 states are occupied by more than 1% in the process.

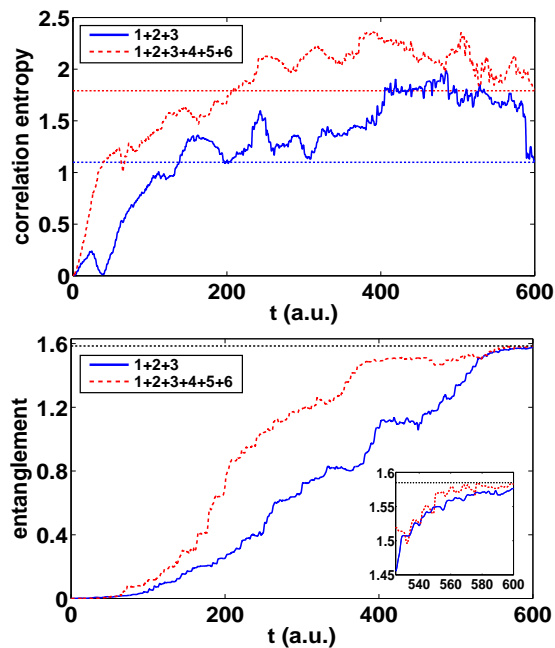


FIG. 5: (color online) Correlation entropy (upper panel) and the entanglement (lower panel) in excitation processes from the ground state the superposition of the first three states (solid lines) and to the superposition of the first six states (dashed lines). The latter process is the same as in Figs. 3 and 4. The horizontal dotted lines in (a) and (b) mark the ideal and maximum values, respectively (see text).

The entanglement in the lower panel of Fig. 5 approaches the theoretical maximum value $\log_2(3) \approx 1.5850$ (dotted line). For the three-state and six-state optimization processes we find 1.5764 and 1.5830, respectively. This can be associated with the *maximization of the entanglement* with 99.5% and 99.9% fidelities, that are comparable to the respective target-state overlaps of 99.5% and 99.6%. Thus, through the proposed setup we are able to find maximally entangled two-electron states in a targeted fashion. We also note that the entanglement could be explicitly measured in the DQD by detecting the charge²⁸ on one of the wells leaving the other well unaffected. This procedure would directly correspond to tracing out one site of the DQD and reducing the density matrix of the whole system to $\rho_j = \text{Tr}_j(|\Psi\rangle\langle\Psi|)$.

We point out three aspects in the practical realization of the proposed control scheme. First, the actual confining potential and thus the Hamiltonian could be determined through a supporting experiment, e.g., by measuring the single-particle spectrum and constructing V_{ext} through inversion.²⁹ The optimization could then be per-

formed within this specific V_{ext} . Secondly, it is important to note that the physical constraints of the optical pulses required to induce the proposed transitions are within reach of the present experimental capabilities. Terahertz frequencies can be routinely produced with, e.g., quantum cascade lasers and they can be shaped even in the femtosecond time scale.³⁰ For example, in a recent experiment³¹ femtosecond pulses were created in a synthesized fashion by separately controlling the infrared, visible, and ultraviolet contributions, including their chirp, carrier envelope phase, delay, and energy (beam size). Therefore, coherent control with THz optics is likely to become a feasible scheme in solid-state quantum information. On the other hand, voltage control with gates is so far strictly limited to GHz time scales. Finally, as the third critical aspect we mention coherence that highly depends on the external conditions in a particular device. We believe that the time scales presented here are coherently reachable, although we cannot rule out the possibility of decoherence due to hyperfine effects or/and interactions with optical and acoustic phonons.

To summarize, we have shown through numerically exact calculations that coupling a two-electron double quantum dot to an optimized optical source enables coherent excitations to entangled states with an extremely high fidelity. In the proposed setup the pulses produced by quantum optimal control theory can be exposed to realistic constraints without losing the accuracy. Time-frequency analysis gives invaluable insight on the physical processes in the evolution towards the desired superposition. We show that entanglement of delocalized and localized electron configurations can be reached up to 99.9% of the theoretical maximum. We hope that the proposed scheme motivates further experiments in the initialization, control, and readout of electric charge in solid-state devices.

Acknowledgments

We thank Robert Westervelt for helpful discussions. M.F.B. and E.J.H. were supported by the Department of Energy, office of basic science (grant DE-FG02-08ER46513), E.R. by the Academy of Finland, the Wihuri Foundation, and the Magnus Ehrnrooth Foundation, and T.B. by Studienstiftung des deutschen Volkes. CSC Scientific Computing Ltd. in Finland and the Odyssey cluster supported by the FAS Science Division Research Computing Group at Harvard University are acknowledged for computational resources.

* Electronic address: esa.rasanen@tut.fi

¹ D. Loss and D. P. DiVincenzo, Phys. Rev. A **57**, 120 (1998).

² For a perspective, see D. P. DiVincenzo, Science **309**, 2173 (2005).

³ J. R. Petta, A. C. Johnson, J. M. Taylor, E. A. Laird, A.

- Yacoby, M. D. Lukin, C. M. Marcus, M. P. Hanson, and A. C. Gossard, *Science* **309**, 2180 (2005).
- ⁴ L. Robledo, J. Elzerman, G. Jundt, M. Atatüre, A. Högele, S. Fält, and A. Imamoglu, *Science* **320**, 772 (2008).
- ⁵ K. C. Nowack, M. Shafiei, M. Laforest, G. E. D. K. Prawiroatmodjo, L. R. Schreiber, C. Reichl, W. Wegscheider, L. M. K. Vandersypen, *Science* **333**, 1269 (2011).
- ⁶ M. D. Shulman, O. E. Dial, S. P. Harvey, H. Bluhm, V. Umansky, and A. Yacoby, *Science* **336**, 202 (2012).
- ⁷ For a review, see R. Hanson, L. P. Kouwenhoven, J. R. Petta, S. Tarucha, L. M. K. Vandersypen, *Rev. Mod. Phys.* **79**, 1217 (2007).
- ⁸ L. Gallmann, C. Cirelli and U. Keller, *Ann. Rev. Phys. Chem.* **63**, 447 (2012).
- ⁹ T. Hayashi, T. Fujisawa, H. D. Cheong, Y. H. Jeong, and Y. Hirayama, *Phys. Rev. Lett.* **91**, 226804 (2003).
- ¹⁰ G. E. Murgida, D. A. Wisniacki, and P. I. Tamborenea, *Phys. Rev. Lett.* **99**, 036806 (2007).
- ¹¹ G. E. Murgida, D. A. Wisniacki, and P. I. Tamborenea, *Phys. Rev. B* **79**, 035326 (2009).
- ¹² N. Sangouard, S. Guerin, M. Amnat-Talab, and H. R. Jauslin, *Phys. Rev. Lett.* **93**, 223602 (2004).
- ¹³ M. Kataoka, M. R. Astley, A. L. Thorn, D. K. L. Oi, C. H. W. Barnes, C. J. B. Ford, D. Anderson, G. A. C. Jones, I. Farrer, D. A. Ritchie, and M. Pepper, *Phys. Rev. Lett.* **102**, 156801 (2009).
- ¹⁴ E. Räsänen, A. Castro, J. Werschnik, A. Rubio, and E. K. U. Gross, *Phys. Rev. B* **77**, 085324 (2008).
- ¹⁵ A. Putaja and E. Räsänen, *Phys. Rev. B* **82**, 165336 (2010).
- ¹⁶ L. Sælen, R. Nepstad, I. Degani, and J. P. Hansen, *Phys. Rev. Lett.* **100**, 046805 (2008).
- ¹⁷ R. Nepstad, L. Sælen, I. Degani, and J. P. Hansen, *J. Phys.: Condens. Mat.* **21**, 215501 (2009).
- ¹⁸ L. E. Jensen, M. T. Bjrk, S. Jeppesen, A. I. Persson, B. J. Ohlsson, and L. Samuelson, *Nano Lett.* **4**, 1961 (2004).
- ¹⁹ E. E. Boyd, K. Storm, L. Samuelson, and R. M. Westervelt, *Nanotechnology* **22**, 185201 (2011).
- ²⁰ A. C. Bleszynski, F. A. Zwanenburg, R. M. Westervelt, A. L. Roest, E. P. A. M. Bakkers, and P. Kouwenhoven, *Nano Lett.* **7**, 2559 (2007).
- ²¹ A. P. Peirce, M. A. Dahleh, and H. Rabitz, *Phys. Rev. A* **37**, 4950 (1988); R. Kosloff, S. A. Rice, P. Gaspard, S. Tersigni, and D. J. Tannor, *Chem. Phys.* **139**, 201 (1989).
- ²² J. Werschnik and E. K. U. Gross, *J. Opt. B: Quantum Semiclass. Opt.* **7**, S300 (2005).
- ²³ A. Castro, H. Appel, M. Oliveira, C. A. Rozzi, X. Andrade, F. Lorenzen, M. A. L. Marques, E. K. U. Gross, and A. Rubio, *Phys. Stat. Sol. (b)* **243**, 2465 (2006).
- ²⁴ A. Castro, E. Räsänen, A. Rubio, and E. K. U. Gross, *Europhys. Lett.* **87**, 53001 (2009).
- ²⁵ P. Ziesche, O. Gunnarsson, W. John, and H. Beck, *Phys. Rev. B* **55**, 10270 (1997).
- ²⁶ Z. Huang, H. Wang, and S. Kais, *J. Mod. Opt.* **53**, 2543 (2006).
- ²⁷ P. Zanardi *Phys. Rev. A* **65**, 042101 (2002).
- ²⁸ M. Field, C. G. Smith, M. Pepper, D. A. Ritchie, J. E. F. Frost, G. A. C. Jones, and D. G. Hasko, *Phys. Rev. Lett.* **70**, 1311 (1993).
- ²⁹ E. Räsänen, J. Könemann, R. J. Haug, M. J. Puska, and R. M. Nieminen, *Phys. Rev. B* **70**, 115308 (2004).
- ³⁰ Y.-S. Lee, *Principles of Terahertz Science and Technology*, Springer, 2009.
- ³¹ A. Wirth, M. Th. Hassan, I. Grguras, J. Gagnon, A. Moulet, T. T. Luu, S. Pabst, R. Santra, Z. A. Alahmed, A. M. Azzeer, V. S. Yakovlev, V. Pervak, F. Krausz, and E. Goulielmakis, *Science* **334**, 195 (2011).